3D PRINTED COMPOSITE MEMBRANES WITH ENHANCED ANTI-FOULING BEHAVIOUR

Abouther Al-Shimmery, Saeed Mazinani, Jing Ji, Y.M. John Chew and Davide Mattia*

Department of Chemical Engineering, University of Bath, Claverton Down, Bath BA2 7AY, UK and

Centre for Advanced Separations Engineering, University of Bath, Claverton Down, Bath BA2 7AY, UK

Corresponding author: d.mattia@bath.ac.uk

Abstract

The fabrication of three dimensional (3D) printed composite membranes by depositing a thin polyethersulfone (PES) selective layer onto ABS-like 3D printed flat and wavy structured supports is presented here for the first time. The 50 mm disk supports were printed using an industrial 3D printer with both flat and double sinusoidal, i.e. wavy, surface structures. The thin selective layers were deposited onto the 3D supports via vacuum filtration. The resulting flat and wavy composite membranes were characterised and tested in terms of permeance, rejection, and cleanability by filtering oil-in-water emulsions of 0.3 - 0.5 vol. % through a cross-flow (Reynolds number, *Re* = 100, 500 and 1000) ultrafiltration set-up under a constant transmembrane pressure of 1 bar. Results showed that pure water permeance through the wavy membrane was 30% higher than the flat membrane for *Re* = 1000. The wavy 3D printed membrane had a 52 % higher permeance recovery ratio compared to the flat one after the first filtration cycle, with both membranes having an oil rejection of 96% ± 3%. The wavy 3D composite membrane maintained some level of permeation after 5 complete filtration cycles using only water as the cleaning/rinsing agent, whereas the flat one was completely fouled after the first cycle. Cleaning with NaOCl after the sixth cycle restored ~70% of the initial permeance for the wavy membrane. These results demonstrate that 3D printed wavy composite membranes can be used to significantly improve permeation and cleanability performance, particularly in terms of reducing fouling build-up, i.e. the main obstacle limiting more widespread adoption of membranes in industrial applications.

keywords: 3D printing; fouling; oil-in-water emulsion; thin film composite; PES

1. Introduction

The push towards minimizing waste and reduce energy consumption in a wide range of industrial processes is driving the replacement of legacy technology with membrane-based processes [1]. However, fouling removal from membranes remains a formidable challenge towards their more widespread adoption as cleaning is costly and generates significant amounts of waste [2]. This is particularly true in the oil industry where there is an urgent need to recover oil from waste process streams, which are often in the form of oil-in-water emulsions with oil concentrations as high as 1000 mg/L [3]. Traditional methods such as gas flotation, use of chemical demulsifiers, skimmers, and electrostatic processes all generate secondary waste streams [4-6], and are not always effective at demulsifying stable emulsions [7]. Although membrane processes are effective at breaking up oil-in-water emulsions [8], they all suffer significantly from fouling, requiring extensive chemical cleaning [9, 10]. Common methods, including using sodium dodecyl sulfate (SDS) [11], micellar solutions of SDS [12], and alkali washing followed by acid washing [13], while effective, all produce secondary waste streams and can, over time, damage the membranes [14].

As a consequence, there is strong interest in novel membrane materials and/or structures that can reduce the build-up of fouling and use of cleaning agents. In all cases, the main goal is to reduce the interactions between the foulants and the membrane surface [15], either by changing the membrane's wetting behaviour [8] or by promoting fluid turbulence at the membrane surface via surface structuring [16]. The latter approach has the advantage of being applicable to commercial membrane materials and is, as such, preferred. Turbulence is primarily achieved by generating vortexes in the vicinity of the membrane surface due to the presence of regular or irregular patterned structures such as pillars [17], lines [18], or indents [19]. These patterns are obtained by using a variety of techniques e.g., micro-moulding [20], nanoimprint lithography [16], or by mixing inorganic fillers in a mixed matrix membrane [21]. In all instances, the structures induce localised turbulence near the membrane's surface, leading to reduced build-up of fouling, with a strong effect of the orientation of the structures vis-à-vis the flow direction [16]. Computational fluid dynamics (CFD) and experiments showed that particle deposition on prism-patterned membranes was mitigated compared to a flat membrane of the same material due to vortex formation in the valley areas [22]. Similar effects were also observed for microbial attachment on a line-patterned polyvinylidene fluoride (PVDF) membrane, with low deposition in high shear regions (i.e. peaks) and high deposition in low shear regions (i.e. valleys) [23]. The effects were similar for BSA fouling on a nanoimprinted membrane, with lower fouling on the patterned membrane compared to a flat one [24].

While being effective, current patterning methods are limited in the types of structures that can be produced on a membrane [25] and the effect the patterning process has on the durability and permeance of the membrane [19, 23]. 3D printing is an emerging membrane fabrication technology that enables the manufacture of more complex and irregular membrane shapes and structures which cannot be

obtained via current methods [26]. There are still few examples of this approach including a 3D printed CO_2-water PDMS contactor, showing higher mass transfer of CO_2 into water compared to a hollow fibre membrane [27]; a 3D printed polysulphone support used to prepare a membrane with switchable wettability surfaces via the coating of candle soot [28]; the combination of ink-jet printing and interfacial polymerization to create thin film composite membranes [29], and the combination of 3D printing and photopolymerization to create patterns atop a commercial ultrafiltration membrane [30].

In this paper, a new approach is presented to generate flat and wavy composite membranes by depositing a thin polyethersulfone (PES) selective layer onto a 3D printed membrane support. The anti-fouling property of the resulting 3D printed composite membrane was tested using oil-in-water emulsions as model foulants, studying the effect of cross-flow velocity and oil concentration on oil rejection and flux recovery. Comparisons between the flat and wavy membranes were made in terms of pure water permeance, oil-in-water emulsion permeance, and four fouling indices namely, permeance recovery ratio, reversible permeance decline ratio, irreversible permeance decline ratio, and total permeance decline ratio.

2. Materials and methods

2.1 Materials

Urethane acrylate oligomers (acrylonitrile butadiene styrene, VisiJet® M3-X, 3D Systems) and a proprietary paraffin wax (VisiJet® S300, 3D Systems) were used by 3D printer (ProJet 3500 HD Max printer, 3D Systems) to fabricate 3D supports. After printing, the support structure was removed with the EZ Rinse – C oil cleaner. All 3D printing materials and removal agents were purchased from 3D Systems. Polyethersulfone (PES, Radel A300, M_w = 15 kDa) and N, N- Dimethylacetamide (DMAc) solvent from Acros organics were used to prepare casting solutions of PES selective layer. Deionized water (Millipore) and pure sunflower oil (purchased from a local supermarket) were used to prepare the oil-in-water emulsions feed solution with different oil concentrations (0.3, 0.4 and 0.5 vol. %). For chemical cleaning of the fouled membranes, sodium hydroxide (NaOH), sodium dodecyl sulfate (SDS) ($NaC_{12}H_{25}SO_4$) and sodium hypochlorite (NaOCl) were purchased from Sigma-Aldrich. The concentration of chemicals used for all cleaning experiments was 0.1 M.

2.2 Preparation of wavy and flat membrane support

There were three main steps in fabricating the 3D printed wavy supports: First, Autodesk Inventor professional 2016 was used to design the porous area, specifying the diameter of the pores, the distance between the pores and the number of pores. The dimensions were converted into codes for the OpenScad program. Second, an open-access code (link) for designing sinusoidal structures was modified by specifying the resolution, the number of peaks, peak height and peak distance. Finally, the pore structure was superimposed onto the wavy surface (37 mm diameter) and a 6.5 mm rim added around the circular

porous area (Fig. 1). The Computer-aided design (CAD) file was converted to a stereolithography format file (STL) and input to the 3D printer (Project 3500 HD Max printer, 3D Systems). In turn, the printer converted the drawing into two dimensional layers (or slices), each with a thickness of 16 µm, which were used to print the supports. Once completed, the build platform was removed from the printer and placed in a refrigerator for 5 min to detach the support from the platform. Thereafter, several methods were tried to remove the wax from the support's pores, with the best results obtained using ultrasonication in EZ Rinse – C oil for 6 hr at 60 °C. Fig. 2a shows the 3D printed support after the cleaning process. A flat 3D support with the same pore structure and footprint as the wavy one was also prepared (Fig. S1). The effective filtration areas for the flat and wavy supports are 1,074 and 1,216 mm^2, respectively, calculated by surface integration using the built-in MATLAB function (meshgrid (x, y)).

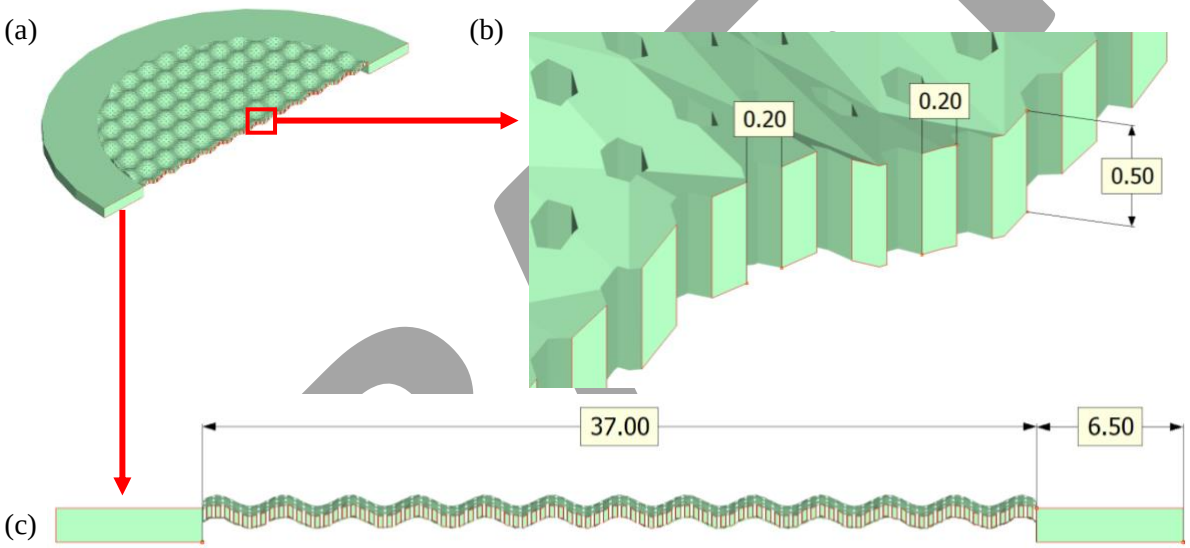

Fig. 1. CAD of 3D wavy support: (a) top view; (b) enlarged cross section; and (c) side view, with amplitude = 0.5 mm, frequency = 2 s^{-1}, and wave length = 3 mm. All dimensions are in mm. The wavy surface is described using the equation $f(x, y) = 0.5 \times \sin(x) \times \sin(y)$.

2.3 Preparation of PES selective layer

The PES dope solution was prepared by first dissolving 15 wt. % of granular PES in 85 wt. % DMAc at room temperature. The mixture was stirred using a roller mixer (SRT6D, Stuart Equipment) at 60 rpm for 48 hours until the PES was completely dissolved, resulting in a yellowish transparent solution. The polymer solution was left for at least 24 hours to release any air bubbles generated during mixing. Phase inversion was used to fabricate the selective layer by casting the polymer solution directly onto a clean glass plate using a casting knife with a gap height of 50 µm at approximately 30% relative humidity and room temperature (19 – 21 °C). The glass plate with the cast film was immediately immersed in a coagulation bath of deionised water at room temperature to initiate the phase separation

process. To remove any traces of DMAc, the membrane was then stored in water for at least 3 days with fresh water replaced every 24 hours.

2.4 Preparation of wavy and flat 3D composite membranes

Fig. 2 summarises the procedure that has been used to prepare the wavy 3D composite membranes. A 3D wavy support is shown in Fig 2a. A piece of PES selective layer with dimensions 7 × 7 cm was cut (Fig. 2b) after checking with a backlit LED light box to identify any damage or holes. An undamaged film was then placed over the 3D support and 250 mbar vacuum pressure (without water) was applied for 1 minute to adhere the selective layer over the 3D support. Then, vacuum filtration with pure water was applied for 30 minutes to increase adherence and stability of the selective layer over the 3D support (Fig. 2c), resulting in a wavy 3D composite membrane (Fig. 2d). The same procedure was followed to make flat 3D composite membranes.

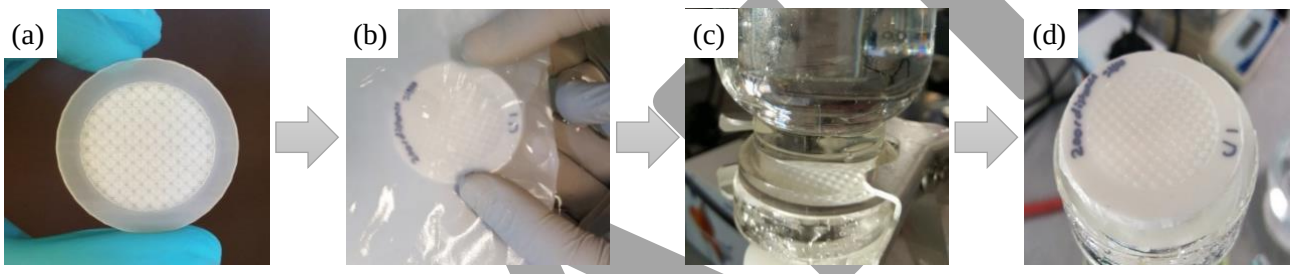

Fig. 2. Preparation of wavy 3D composite membranes: (a) 3D wavy support; (b) PES thin layer is laid over the wavy support; (c) vacuum filtration to adhere the selective layer onto the support; and (d) resulting 3D composite membrane.

2.5 Characterisations of wavy and flat 3D composite membranes

Scanning electron microscopy (JEOL FESEM6301F) was used to characterise the morphology of the 3D support and selective layer. Samples were fractured in liquid nitrogen and then coated with gold. The film thickness of PES membrane was quantified from analysis of SEM micrographs at different locations using Image J and the average value was recorded. The topography of the 3D support and composite membrane was imaged using a digital microscope (VHX – 6000, Japan). A contact angle goniometer (OCA machine, Data Physics, Germany) was used to measure the water and oil contact angles on the 3D support and composite membrane at room temperature. 5 µL droplets of water or sunflower oil were used and the values reported are the average of ten measurements in different positions. Membrane resistance was determined using the procedure reported in [31]. The porosity of the selective layer was measured by the gravimetric method, using the following equation [32]:

$$porosity\ (\varepsilon) = \frac{W_w - W_d}{\rho_w \times V_a} \times 100 \qquad (1)$$

where W_w is the weight of the wet membrane, W_d is the weight of the dry membrane, ρ_w is the pure water density and V_a is the volume of selective layer. A 3 cm diameter circular piece of selective layer was soaked in pure water at room temperature for 24 h. The membrane was then taken out and its wet

weight directly recorded after removing the excess surface water with a tissue. The selective layer was then put in a vacuum oven for 6 h at 65 °C to obtain the dry weight. Four samples were measured and the average value is reported.

The POROLUX-1000 was used to measure the average pore size of the selective layer.

2.6 Emulsions preparation and characterization

The oil-in-water emulsion was prepared by adding specific amounts of oil in one liter of water (0.3, 0.4, and 0.5 vol. %). A homogenizer (ULTRA-TURRAX, T 25 basic, IKA) was used to mix the oil with water at 19,000 rpm for 5 minutes. A master sizer (Malvern) was used to determine the size distribution of the oil droplets.

2.7 Membrane preparation and characterization

Ultrafiltration experiments were carried out using a recirculating cross-flow setup (Fig. S2). Each membrane was first pre-compacted with pure water at 1.5 bar for 2-3 h until the water permeance reached a steady value. The permeance (K, LMH bar^{-1}) and oil rejection percentage (R, %) were calculated using the following equations:

$$K = \frac{V}{\Delta t \times A \times \Delta p} \quad (2)$$

$$R\ (\%) = \frac{C_F - C_P}{C_F} \quad (3)$$

$$R_m = \frac{1}{K\mu} \quad (4)$$

where V is the volume of permeate (m^3) over time Δt (hr); A is the effective membrane area (m^2) for the flat and wavy membranes (cfr. Section 2.2); Δp is the transmembrane pressure (bar); C_F is the oil concentration in the feed solution (mg/L) and C_P is the oil concentration on the permeate side (mg/L); μ is the viscosity and R_m is the hydraulic resistance (m^{-1}). A turbidity meter (EUTECH TN-100, Thermo-Scientific) was used to determine the oil concentration in the feed and permeate [33]. Three feed flow rates (0.14, 0.7 and 1.4 L min^{-1}), corresponding to Reynolds number Re = 100, 500 and 1000, were used in the filtration experiments. The oil-in-water emulsion was initially calibrated for different known oil concentrations in terms of the intensity of scattered light in the water in units of turbidity NTU (nephelometric turbidity units). The relationship between the intensity of scattered light and the oil concentration was linear with $R^2 = 0.99$. The generated equation was used to measure the unknown oil concentration (Fig. S3). For all experiments the average from three replicate tests is reported.

The antifouling behaviour of the membranes was assessed using the following procedure: First, a 3D composite membrane was pressurized at 1.5 bar for 2-3 hours until it reached steady state (pre-compaction). Oil-in-water emulsions with different oil concentration (0.3, 0.4 and 0.5 vol. %) were then

used as feed solution and repeat cycles of filtrations (fouling – cleaning) were performed (Fig. 3). All fouling and cleaning experiments were performed at a constant transmembrane pressure of 1 bar. For each cycle, the initial pure water permeance, $P_{w,i}$, was recorded for 30 minutes. The oil-in-water emulsion was then flowed through the crossflow cell until the permeance, $P_{E,i}$, reached steady state (90 minutes). The cleaning step was performed by flowing pure water at the same operating conditions for 15 minutes. After the cleaning step, the recovered pure water permeance, $P_{W,i+1}$, was measured for 30 minutes. The fouling and cleaning cycle was then repeated up to 6 times. To keep the oil concentration in the feed constant, the feed solution was replaced with new emulsion at the start of every new cycle. A magnetic stirrer rotating at a constant rate (480 rpm) was used to prevent the oil droplets from coalescing in the feed for the whole duration of the tests. For all experiments the average values from three replicate tests are reported.

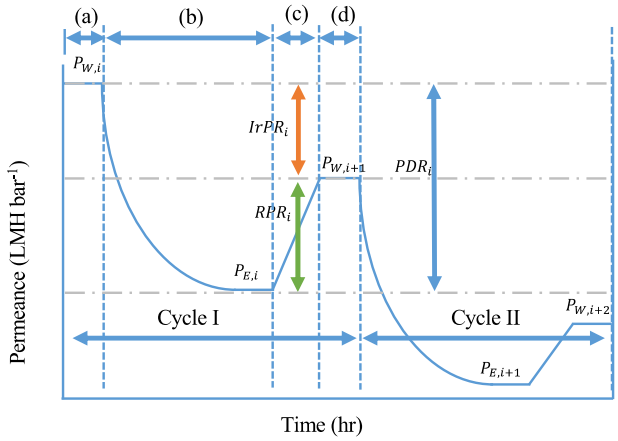

Fig. 3. Schematic of the filtration (fouling-cleaning) cycle: (a) Pure water permeance ($P_{W,i}$) recorded for 30 minutes, (b) oil-in-water emulsion permeance ($P_{E,i}$) recorded for 90 minutes, (c) cleaning with pure water for 15 minutes, (d) pure water permeance ($P_{W,i+1}$) for 30 minutes. The transmembrane pressure was maintained at 1 bar throughout the fouling-cleaning cycle.

Four fouling indices namely, permeance recovery ratio, PRR_i, reversible permeance decline ratio, RPR_i, irreversible permeance decline ratio, $IrPR_i$, and total permeance decline ratio, PDR_i, the sum of the previous two quantities, were calculated to evaluate the anti-fouling property of the membranes during each cycle using the equations (5) to (8) [40]:

$$PRR_i\ (\%) = \left(\frac{P_{W,i+1}}{P_{W,i}}\right) \times 100 \tag{5}$$

$$RPR_i(\%) = \left(\frac{P_{W,i+1} - P_{E,i}}{P_{W,i}}\right) \times 100 \tag{6}$$

$$IrPR_i(\%) = \left(\frac{P_{W,i} - P_{W,i+1}}{P_{W,i}}\right) \times 100 \tag{7}$$

$$PDR_i(\%) = \frac{P_{W,i} - P_{E,i}}{P_{W,i}} \times 100 \quad (8)$$

where i the cycle number. All symbols are indicated on Fig. 3.

2.8 Chemical cleaning

After 6 cycles of fouling-cleaning using only pure water, the membranes were cleaned using 0.1 M of NaOH, SDS or NaOCl for 1 h at a transmembrane pressure of 1 bar and Re =1000, followed by washing with pure water for 15 minutes (to remove any chemical residue) at the same operating conditions. Then, the pure water permeance was measured for 30 minutes. This process was repeated for the flat 3D composite membrane after the 2nd cycle.

3. Results and discussion

3.1 Characterization of support, selective layer and 3D composite membranes

The topographical analysis using a digital microscope of the 3D printed supports shows regular distribution of the pores in the wavy structure (Fig. 4a), and that the pores are indeed open (Fig. 4b).

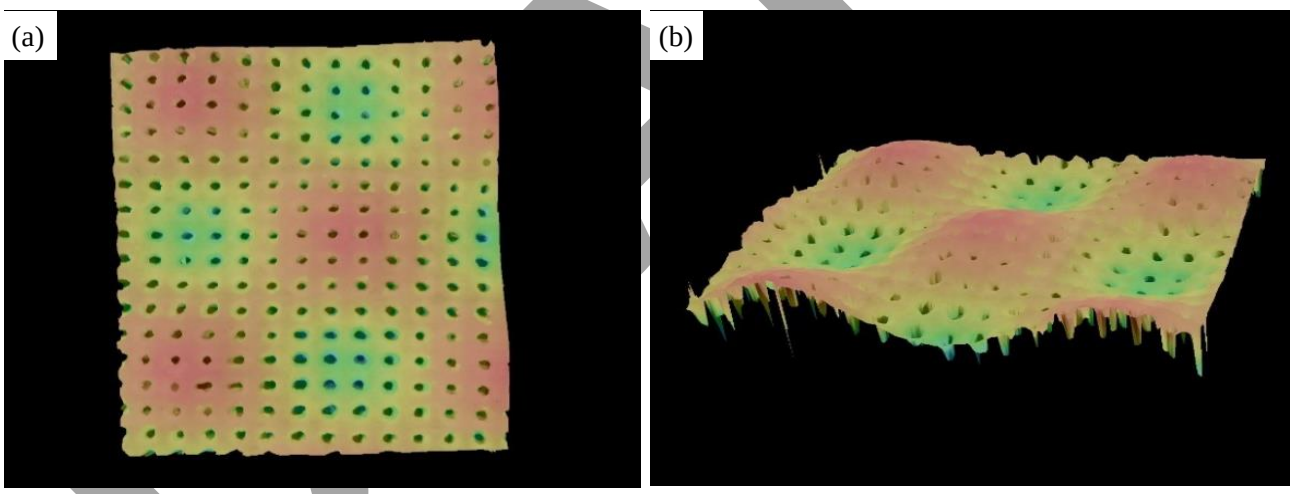

Fig. 4. Digital micrographs of the wavy support showing (a) a regular structure (top view) and (b) open porosity (side view). The color map represents height with red indicating peaks and green valleys. Pore diameter = 0.2 mm, distance between pores = 0.2 mm, amplitude = 0.5 mm, frequency = 2 s^{-1}, and wave length = 3 mm.

The design parameters for the 3D printed support have been optimised based on a systematic investigation of the resolution of the 3D printer, the material's mechanical properties and the amount of turbulence generated by the features. The first significantly affected pore diameter and interpore distance: While the printer's nominal resolution is 16 μm, it was observed that printing features sizes less than 200 μm did not result in regular, open and circular pores, as in the present case (Fig. 4). The material's mechanical properties dictated the minimum thickness of the 3D printed support (Fig. 1c), below which the support was not able to withstand any significant pressure. The double sinusoidal design (amplitude, frequency, wavelength) was determined

by CFD simulations showing that higher amplitude, increased frequency and shorter wavelengths would generate increased turbulence (Fig. S4). At the same time, though, it was observed that when the features were too sharp, the selective layer would not conform to the support's shape or be pierced through during the vacuum-driven adhesion step, resulting in the optimised values used in the present work (amplitude = 0.5 mm, frequency = 2 s^{-1}, and wave length = 3 mm).

The surface of the PES selective layer is smooth, with no visible pin-holes at 20,000 magnification (Fig. 5a). The cross section of the layer shows a typical asymmetric structure membrane with a finger-like porous sublayer and a ~ 500 nm dense top layer (Fig. 5b) with a total thickness of 16 ± 1 µm (analysis of the SEM micrographs was carried out using Image J).

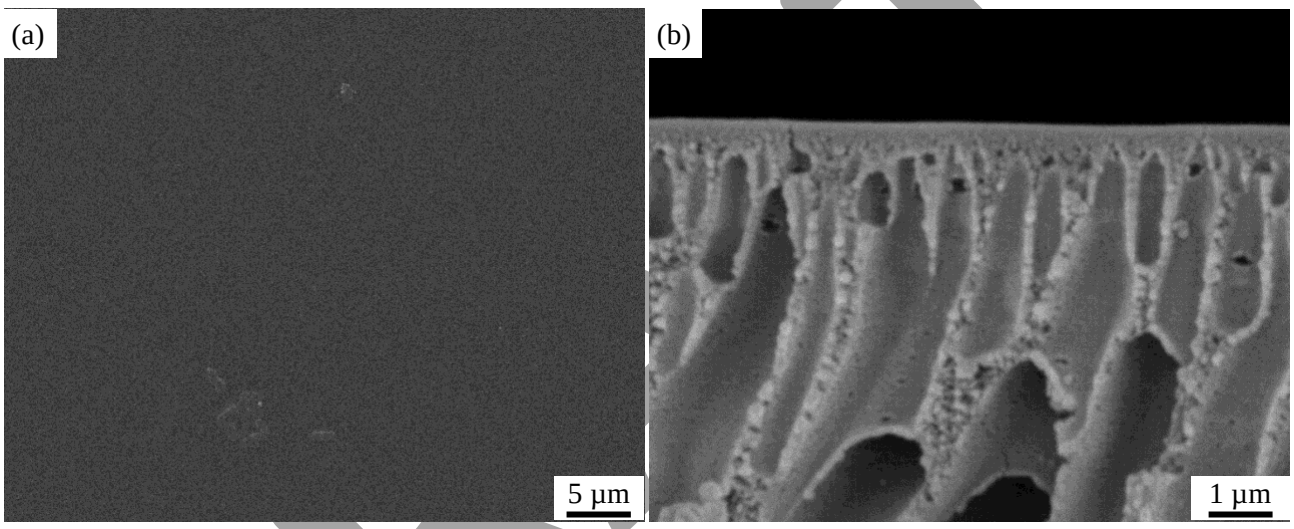

Fig. 5. SEM micrographs of PES selective layer: (a) top surface and (b) cross section.

SEM micrographs of the wavy 3D composite membrane show that it retains the wavy structure of the underlying printed support (Fig. 6a), including the latter's triangular facets (Fig. 6b), an indication of a good adhesion between the selective layer and the support. This is further reflected in the topographical image obtained by digital microscopy where peaks are shown in red and the valleys in green (Fig. 6c). Table 1 shows a summary of the physico-chemical characteristics of the 3D printed supports and the PES selective layer. The latter's porosity and average pore size are comparable with values for other ultrafiltration PES selective layers prepared using 15% polyethersulfone [34, 35], whereas the hydraulic resistance is towards the higher end of values found in the literature [36]. The roughness of the composite membrane was 67 nm, slightly less than that of the support, but significantly higher than the stand-alone PES layer. This is further confirmation of the good adhesion of the PES layers onto the support.

Table 1. Physical properties of wavy 3D composite membrane

	porosity	av. pore size	thickness	roughness, Ra	R_m	contact angle
	%	nm	μm	nm	m^{-1}	deg
PES film	70	54 ± 10	16 ± 1	3.1	$0.55*10^{16}$	63 ± 2
flat support	76†	2000	500	73	$1.6*10^{12}$	83 ± 2
wavy support						

† from model.

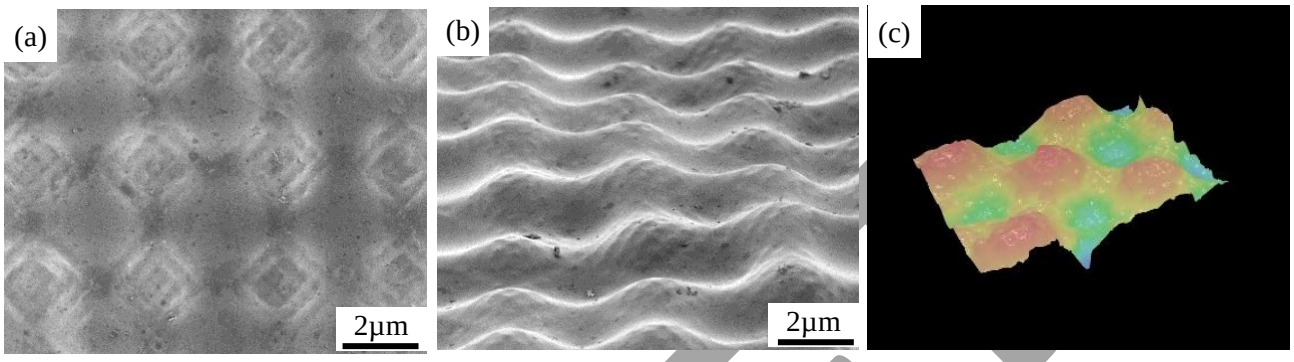

Fig. 6. SEM micrographs of 3D composite membrane, (a) top view, (b) side view, and (c) 3D topographic optical image.

3.2 Permeance – rejection performance

Crossflow filtration cycles were first conducted on the flat 3D composite membrane, with any appreciable flux for the oil-in-water emulsion, observed only when tested at Re = 1000 (Fig.7). Even at this high value, the membrane fouled rapidly, with no measurable permeance recovery after cleaning with water.

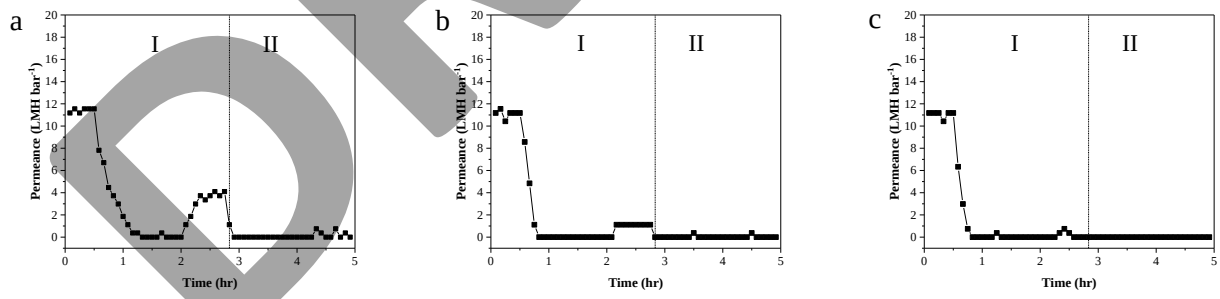

Fig. 7. Variation of permeance with time during crossflow filtration of flat 3D composite membranes for Re = 1000 and as a function of oil concentration (a = 0.3 vol. %, b = 0.4 vol. %, c = 0.5 vol. %). In all cases Δp = 1 bar. Regions identified by roman numerals I and II represent the first and second cycle. Each data point is the average of 3 repeats on different membranes from the same batch, with an average error of ± 0.1 LMH bar^{-1} (error bars are not shown for clarity).

For the wavy 3D composite membrane, the behavior was significantly different from the flat one: The pure water permeance, P_W, increases with increasing crossflow velocity, from ~11 LMH bar^{-1} at Re = 100 to ~16 LMH bar^{-1} for Re = 1000 (the corresponding crossflow velocity values are 0.014 and 0.14 m/s, respectively). At the highest crossflow velocity, the wavy 3D composite membrane has a ~30%

higher P_W compared to the flat one (cfr. Fig.s 7a and 8g). This is attributed to the 13% higher effective surface area of the former compared to the latter, given by the wavy structure, while retaining the same footprint (50 mm diameter). This increase highlights a key advantage of using 3D structured membranes, whose surface area could be further enhanced by optimizing the wavy structure design: For example, increasing the peak amplitude from 0.5 to 0.75 mm (cfr. Fig.1), would lead to an increase in the surface area of wavy to flat membrane from 13 to 27 % (not shown here).

When the feed was switched from pure water to the oil-in-water emulsion, a sharp decline in permeance was observed, for all crossflow velocities and oil concentrations, as expected. The permeance decline was observed during the initial 30 minutes from the switch. The permeance values then reached approximately steady state after the next hour. The decline can be attributed to the affinity between the oil droplets and membrane surface due to the low hydrophilicity of PES (contact angle = 63° ± 2), and fouling of the surface by the oil [37, 38]. After the first cycle (pure water → oil-in-water emulsion (fouling) → pure water (cleaning)), a second fouling-cleaning cycle was performed, with no chemical cleaning nor interruption between the two. A very stark difference can be observed between the flat and wavy 3D composite membranes, with 37% permeance recovery ratio for the former and 89% for the latter for Re = 1000 and oil concentration = 0.3 vol. % (Table 2).

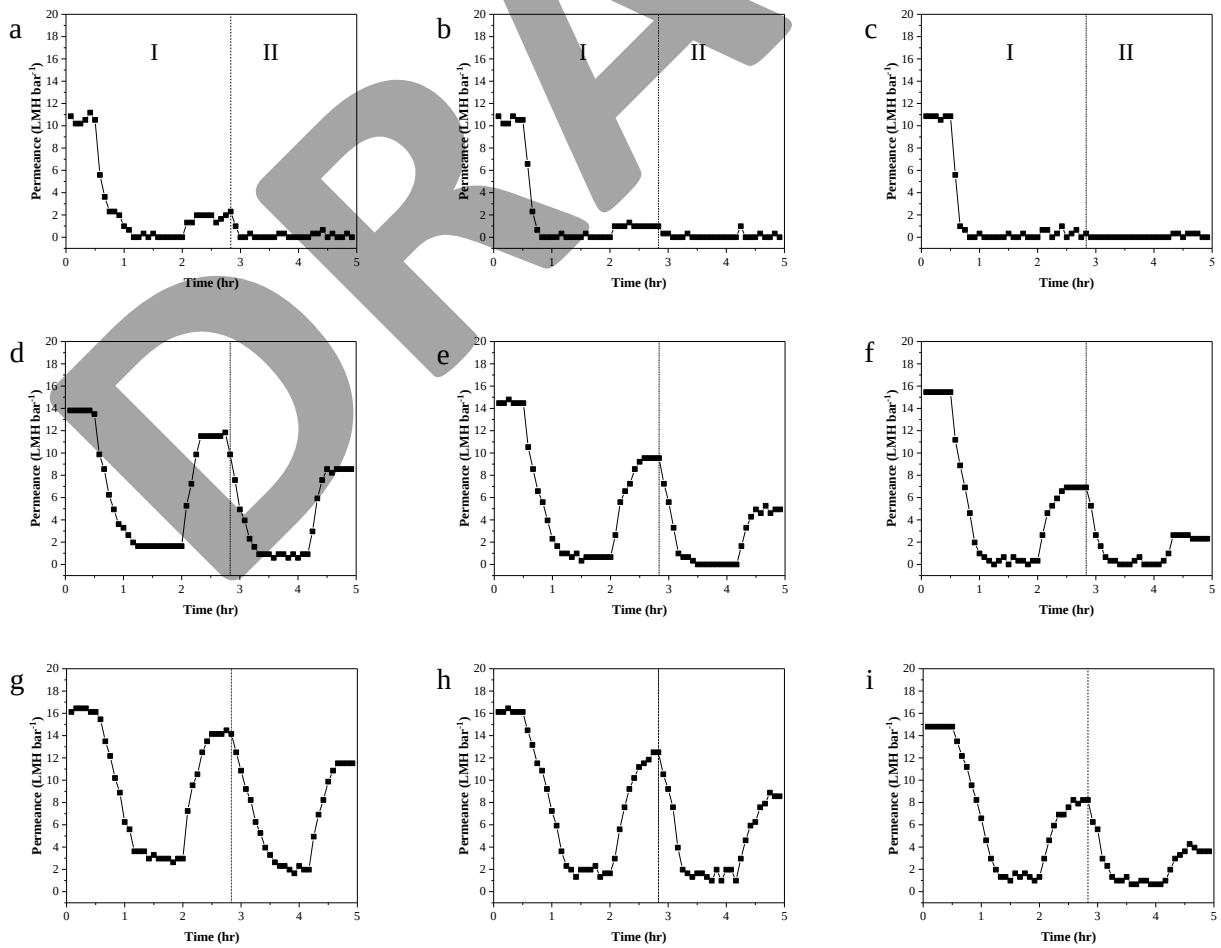

Fig. 8. Variation of Permeance with time during crossflow filtration of wavy 3D composite membranes as a function of Reynolds numbers (Re = 100, 500, 1000 for top, middle and bottom row, respectively) and oil concentration (a, d, g = 0.3 vol. %, b, e, h = 0.4 vol. %, c, f, i = 0.5 vol. %). In all cases Δp = 1 bar. Regions identified by roman numerals I and II represent the first and second cycle. Each data point is the average of 3 repeats on different membranes from the same batch, with an average error of ± 0.8 LMH bar^{-1} (error bars are not shown for clarity).

A high oil rejection (96% ± 3%) was achieved for both the flat and wavy 3D composite membranes (Table 2), with the permeate appearing completely clear (Fig. S5). This can be ascribed to the fact that the average oil droplet diameter (9.9 µm) was significantly larger than the average membrane pore size (54 ± 10 nm).

Table 2. Performance indicators for wavy and flat 3D composite membrane at Re = 1000 and 0.3 vol. % oil concentration for the first complete cleaning cycle.

	P_W	P_E	Oil rejection	PRR	RPR	IrPR	PDR
	LMH bar^{-1}	LMH bar^{-1}			%		
flat	11 ± 0.9	~ 0	96 ± 3	37 ± 2.7	37 ± 0.3	63 ± 2.7	100 ± 3
wavy	16 ± 0.5	3 ± 0.8		89 ± 2.7	71 ± 0.3	10.1 ± 2.7	81 ± 3

In terms of fouling performance, the flat 3D composite membrane had a permeance decrease ratio close to 100% (Table 2 and Fig. 9), with a large irreversible fouling component (63%). Furthermore, fouling of the flat 3D composite membrane at the end of the second cycle is virtually all irreversible, with no permeance.

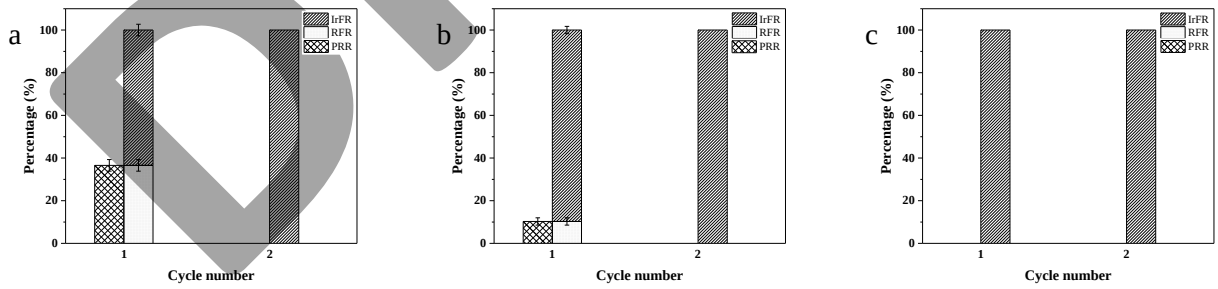

Fig.9. PRR, and PDR (sum of RPR and IrPR) during crossflow filtration of flat 3D composite membranes for Re = 1000 and as a function of oil concentration (a = 0.3 vol. %, b = 0.4 vol. %, c = 0.5 vol. %). In all cases Δp = 1 bar. Each data point is the average of 3 repeats on different membranes from the same batch

For the wavy 3D composite membrane, the permeance recovery ratio (PRR) between the first and second cycle increased significantly with increasing crossflow velocity, from ~18 to ~89 % when the Reynolds number increased from 100 to 1000 for the lowest oil concentration (cfr Fig.s 10a and 10g). The corresponding PRR value for the flat 3D composite membrane at *Re* = 1000 is less than ~37 % (Fig. 9a and Table 2). At the

highest oil concentration, there was virtually no recovery for the lowest crossflow velocity (Fig. 10c) and a decrease from ~88 to ~55 % for the highest crossflow velocity for the wavy 3D composite membrane (cfr. Fig.s 10g and 10i). The PRR of the wavy 3D composite membrane well compares to literature values for pure PES membranes, including a 56 % recovery ratio with comparable oil rejection for a 0.1 vol. % gas oil-in-water emulsion in cross-flow at 4.65 L min^{-1} and Δp = 1.5 bar [39]; and a 69 % recovery ratio for and 0.1 vol. % vacuum oil-in-water emulsion in dead-end configuration [38]. The addition of co-polymers [38] or inorganic fillers [39] to pure PES or the use of chemical cleaning agents [11] can significantly improve the recovery ratio to above 99%. An in-depth analysis of PES membranes used for oil-in-water separation can be found in Table S1, where emsulsions with heavier oils, approaching produced water from oil extraction, have been investigated.

The PRR of the wavy 3D composite membrane at the end of the second cycle showed a modest decrease with increasing oil concentration, going from ~88 to ~80 %, for Re = 1000 and 0.3 vol. % oil concentration (Fig. 10g).

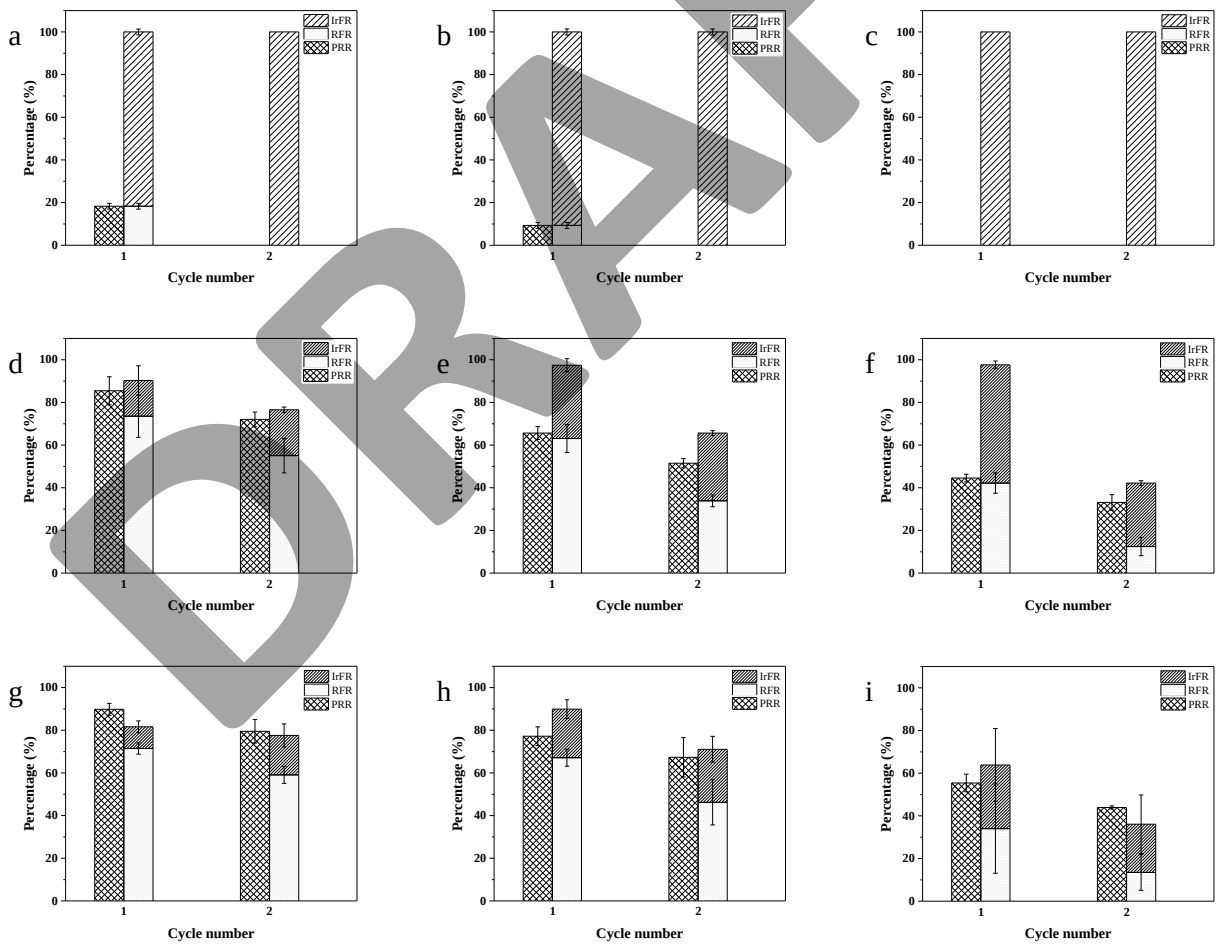

Fig. 10. PRR and PDR (sum of RPR and IrPR) during crossflow filtration of wavy 3D composite membranes as a function of Reynolds numbers (Re = 100, 500, 1000 for top, middle and bottom row, respectively) and oil concentration (a, d, g = 0.3 vol. %, b, e, h = 0.4 vol. %, c, f, i = 0.5 vol. %). In all cases Δp = 1 bar. Each data point is the average of 3 repeats on different membranes from the same batch.

In the case of the flat 3D composite membrane at Re = 1000, there was no recovery after the second cycle or for higher oil concentrations (Fig. 9a-c). These divergent behaviours can be convincingly attributed to the localized turbulence generated by the patterned structure [19, 23]. It should be noted here that there is no chemical cleaning between the two cycles. Hence, the permeance recovery can be entirely attributed to hydrodynamics effects associated with vortices generated between the peaks of membrane surface, which remove the oil from the membrane surface. The decrease in PRR with increasing oil concentration further supports this idea, as the thicker the oil layer over the membrane surface the harder it is to remove it entirely by pure water flushing alone [40]. The total permeance decline ratio (PDR) reported in Fig.s 9 and 10 for the flat and wavy 3D composite membranes, respectively, is the sum of the reversible (RFR) and irreversible (IrFR) permeate decline ratios. The former is associated with the formation of a continuous oil layer forms over the surface of the membrane as a result of droplets accumulation on the surface followed by migration and coalescence [37], whereas the latter corresponds to the oil droplets entering the membranes and depositing inside the pores, leading to permanent fouling of the membrane [41].

The fouling behavior of the wavy 3D composite membrane was further probed for up to 6 cycles of pure water / oil-in-water emulsion filtration / pure water cleaning, followed by a final chemical cleaning, all for Re = 1000. The permeance recovery ratio and the reversible permeate decline ratio declined with the number of cycles, with the P_W and PRR both approaching zero after the 5^{th} cycle for the highest oil concentration (Fig. 11c), and, conversely, with the IrFR reaching around 100 %, (Fig. 11c). It is noted that, in comparison, the flat 3D composite membrane reached the same values after the first cycle for Re = 1000 and oil concentration = 0.3 vol. % (Table 2).

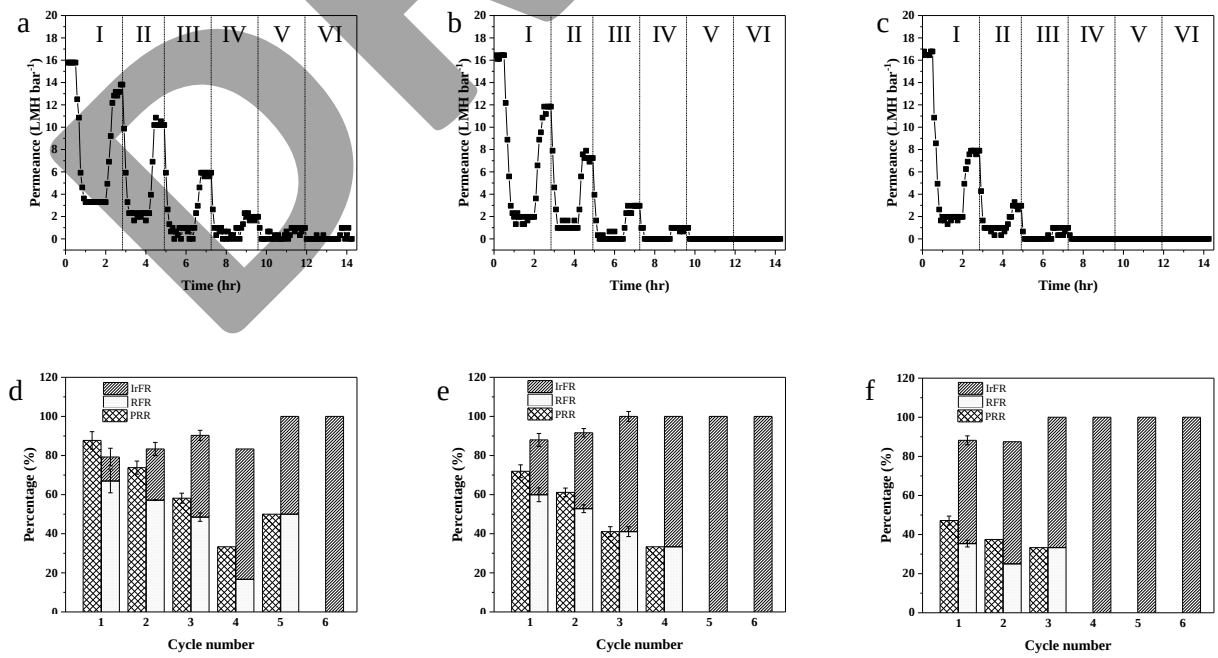

Fig. 11. Variation of Permeance (a, b, c) and PRR, and PDR (sum of RPR and IrPR) (d, e, f) with time during crossflow filtration of wavy 3D composite membrane for Re = 1000 and as a function of oil concentration (a, d = 0.3 vol. %, b, e = 0.4 vol. %, c, f = 0.5 vol. %). In all cases Δp = 1 bar. Regions identified by roman numerals represent the 6 complete filtration cycle. Each data point is the average of 3 repeats on different membranes from the same batch, (average error of ± 0.8 LMH bar^{-1} for a, b, c - error bars are not shown for clarity).

After the sixth cycle, the wavy 3D composite membranes were subjected to three different chemical cleaning agents, i.e. NaOH, SDS, and NaOCl (Fig. 12 a). In all cases, the PRR was significantly higher than the one achievable by using pure water alone. The maximum PRR was around 70 % when the NaOCl was used, while the NaOH showed the weakest cleaning performance with PRR of around 48%. SDS had a moderate effect with PRR of around 63%. The better performance of NaOCl can be attributed to its strong oxidative nature, leading to increased hydrophilicity, which, in turn, reduces the interaction force between the foulants and membrane surface [42]. To investigate the effect of waviness on the chemical cleaning performance, a flat 3D composite membrane was cleaned using 0.1 M NaOCl after two complete filtration cycles with a PRR of ~55 % compared to ~75% for the wavy one (Fig. 12 b). This different behaviour can be attributed to an increase in the diffusion rate of the cleaning agent into the fouling layer induced by the turbulence generated by the wavy structure [43].

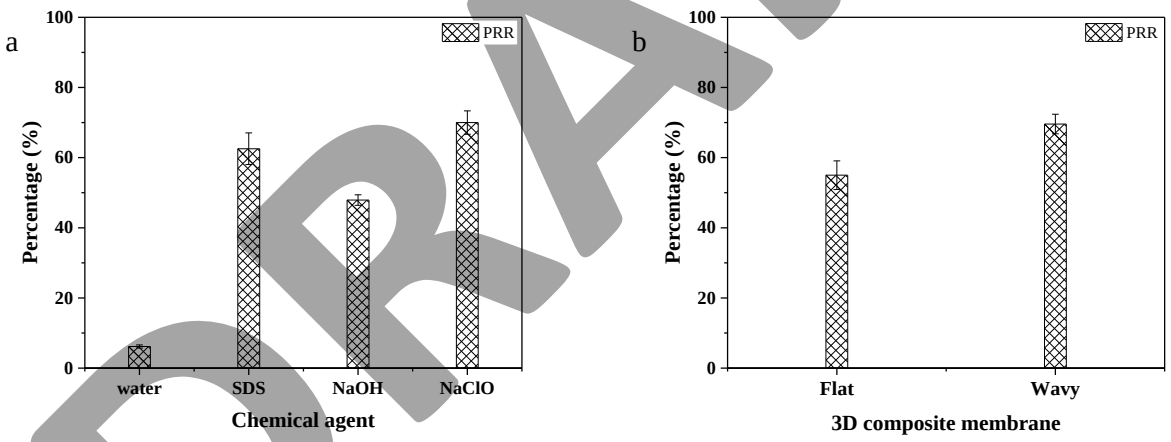

Fig.12. PRR (a) after chemical cleaning using different chemical agents, all at 0.1 M, for a wavy 3D composite membrane after the 6th filtration cycle, and (b) for flat and wavy 3D composite membrane after the 2nd filtration cycle.

4. Conclusions

In this work, a novel thin film composite membrane was successfully fabricated by depositing a PES selective layer onto a 3D printed support. The double-sinusoidal, or wavy, pattern of the support imparted an increase of 30% in pure water permeance and 52% higher permeance recovery ratio compared to a membrane with the same selective layer but flat 3D printed support. The former is the result of a higher effective area with the same overall footprint (50 mm disk), while the latter is due to the increased turbulence generated near the membrane surface by the wavy structure. The wavy 3D

membrane still had permeation after 5 complete filtration cycles using water as the only cleaning agent, compared to the flat one which was completely fouled after the first cycle. Cleaning with NaOCl after the sixth cycle restored ~70% of the initial permeance of the wavy membrane. These membranes significantly outperform literature results of pure PES membranes and are comparable to PES mixed matrix membranes or PES-co-polymer membranes. The low irreversible fouling and the slow fouling build-up of the 3D printed membranes opens the way to significantly lower operational costs for membrane processes as well as reduction in the need for costly and environmental harmful chemical cleaning.

Acknowledgements

The work is supported by Programme Grant EP/M01486X/1 (SynFabFun) funded by the Engineering and Physical Sciences Research Council (EPSRC) UK. A. A.-S. acknowledges the financial support of the Ministry of Higher Education and Scientific Research of Iraq. The authors are grateful to Dr. Darrell Patterson, Dr. Ze Xian Low, and Daniel Scott for fruitful discussions and Nicholas Marsh, Keyence UK Ltd, for providing the images in Fig. 4 and 6c.

All data created during this research are openly available from the University of Bath data archive at: https://doi.org/10.15125/BATH-00571

References

[1] D.S. Sholl, R.P. Lively, Seven chemical separations to change the world, in: Nature, 2016, pp. 435-437.

[2] Y. Wei, H. Qi, X. Gong, S. Zhao, Specially Wettable Membranes for Oil–Water Separation, Advanced Materials Interfaces, 0 1800576.

[3] H.J. Tanudjaja, V.V. Tarabara, A.G. Fane, J.W. Chew, Effect of cross-flow velocity, oil concentration and salinity on the critical flux of an oil-in-water emulsion in microfiltration, Journal of Membrane Science, 530 (2017) 11-19.

[4] R. Moosai, R.A. Dawe, Gas attachment of oil droplets for gas flotation for oily wastewater cleanup, Separation and purification technology, 33 (2003) 303-314.

[5] R. Mohammed, A. Bailey, P. Luckham, S. Taylor, Dewatering of crude oil emulsions 3. Emulsion resolution by chemical means, Colloids and Surfaces A: Physicochemical and Engineering Aspects, 83 (1994) 261-271.

[6] S. Maiti, I. Mishra, S. Bhattacharya, J. Joshi, Removal of oil from oil-in-water emulsion using a packed bed of commercial resin, Colloids and Surfaces A: Physicochemical and Engineering Aspects, 389 (2011) 291-298.

[7] M.-J. Um, S.-H. Yoon, C.-H. Lee, K.-Y. Chung, J.-J. Kim, Flux enhancement with gas injection in crossflow ultrafiltration of oily wastewater, Water research, 35 (2001) 4095-4101.

[8] M. Padaki, R. Surya Murali, M.S. Abdullah, N. Misdan, A. Moslehyani, M.A. Kassim, N. Hilal, A.F. Ismail, Membrane technology enhancement in oil–water separation. A review, Desalination, 357 (2015) 197-207.

[9] S. Kasemset, A. Lee, D.J. Miller, B.D. Freeman, M.M. Sharma, Effect of polydopamine deposition conditions on fouling resistance, physical properties, and permeation properties of reverse osmosis membranes in oil/water separation, Journal of Membrane Science, 425-426 (2013) 208-216.

[10] I.W. Cumming, R.G. Holdich, I.D. Smith, The rejection of oil by microfiltration of a stabilised kerosene/water emulsion, Journal of Membrane Science, 169 (2000) 147-155.

[11] W. Chen, J. Peng, Y. Su, L. Zheng, L. Wang, Z. Jiang, Separation of oil/water emulsion using Pluronic F127 modified polyethersulfone ultrafiltration membranes, Separation and Purification Technology, 66 (2009) 591-597.
[12] S. Lee, Y. Aurelle, H. Roques, Concentration polarization, membrane fouling and cleaning in ultrafiltration of soluble oil, Journal of Membrane Science, 19 (1984) 23-38.
[13] M. Hlavacek, Break-up of oil-in-water emulsions induced by permeation through a microfiltration membrane, Journal of membrane science, 102 (1995) 1-7.
[14] R. Zolfaghari, A. Fakhru'l-Razi, L.C. Abdullah, S.S. Elnashaie, A. Pendashteh, Demulsification techniques of water-in-oil and oil-in-water emulsions in petroleum industry, Separation and Purification Technology, 170 (2016) 377-407.
[15] Y. Ding, S. Maruf, M. Aghajani, A.R. Greenberg, Surface patterning of polymeric membranes and its effect on antifouling characteristics, Separation Science and Technology, 52 (2017) 240-257.
[16] S.H. Maruf, L. Wang, A.R. Greenberg, J. Pellegrino, Y. Ding, Use of nanoimprinted surface patterns to mitigate colloidal deposition on ultrafiltration membranes, Journal of membrane science, 428 (2013) 598-607.
[17] W. Choi, E.P. Chan, J.-H. Park, W.-G. Ahn, H.W. Jung, S. Hong, J.S. Lee, J.-Y. Han, S. Park, D.-H. Ko, Nanoscale pillar-enhanced tribological surfaces as antifouling membranes, ACS applied materials & interfaces, 8 (2016) 31433-31441.
[18] J.W. Bae, Y.-H. Cho, Y.-E. Sung, K. Shin, J.Y. Jho, Performance enhancement of polymer electrolyte membrane fuel cell by employing line-patterned Nafion membrane, Journal of Industrial and Engineering Chemistry, 18 (2012) 876-879.
[19] D.-C. Choi, S.-Y. Jung, Y.-J. Won, J.H. Jang, J.-W. Lee, H.-R. Chae, J. Lim, K.H. Ahn, S. Lee, J.-H. Kim, Effect of Pattern Shape on the Initial Deposition of Particles in the Aqueous Phase on Patterned Membranes during Crossflow Filtration, Environmental Science & Technology Letters, 4 (2017) 66-70.
[20] L. Vogelaar, J.N. Barsema, C.J. van Rijn, W. Nijdam, M. Wessling, Phase separation micromolding—PSμM, Advanced materials, 15 (2003) 1385-1389.
[21] R.J. Gohari, W. Lau, T. Matsuura, A. Ismail, Effect of surface pattern formation on membrane fouling and its control in phase inversion process, Journal of membrane science, 446 (2013) 326-331.
[22] Y.-J. Won, S.-Y. Jung, J.-H. Jang, J.-W. Lee, H.-R. Chae, D.-C. Choi, K.H. Ahn, C.-H. Lee, P.-K. Park, Correlation of membrane fouling with topography of patterned membranes for water treatment, Journal of Membrane Science, 498 (2016) 14-19.
[23] Y.K. Lee, Y.-J. Won, J.H. Yoo, K.H. Ahn, C.-H. Lee, Flow analysis and fouling on the patterned membrane surface, Journal of membrane science, 427 (2013) 320-325.
[24] M. Xie, W. Luo, S.R. Gray, Surface pattern by nanoimprint for membrane fouling mitigation: Design, performance and mechanisms, Water research, 124 (2017) 238-243.
[25] O. Heinz, M. Aghajani, A.R. Greenberg, Y. Ding, Surface-patterning of polymeric membranes: fabrication and performance, Current Opinion in Chemical Engineering, 20 (2018) 1-12.
[26] Z.-X. Low, Y.T. Chua, B.M. Ray, D. Mattia, I.S. Metcalfe, D.A. Patterson, Perspective on 3D printing of separation membranes and comparison to related unconventional fabrication techniques, Journal of Membrane Science, 523 (2017) 596-613.
[27] T. Femmer, A.J. Kuehne, J. Torres-Rendon, A. Walther, M. Wessling, Print your membrane: Rapid prototyping of complex 3D-PDMS membranes via a sacrificial resist, Journal of Membrane Science, 478 (2015) 12-18.
[28] S. Yuan, D. Strobbe, J.-P. Kruth, P. Van Puyvelde, B. Van der Bruggen, Super-hydrophobic 3D printed polysulfone membranes with a switchable wettability by self-assembled candle soot for efficient gravity-driven oil/water separation, Journal of Materials Chemistry A, 5 (2017) 25401-25409.
[29] S. Badalov, Y. Oren, C.J. Arnusch, Ink-jet printing assisted fabrication of patterned thin film composite membranes, Journal of Membrane Science, 493 (2015) 508-514.

[30] Y.M.J. Chew, W.R. Paterson, D.I. Wilson, Fluid dynamic gauging: A new tool to study deposition on porous surfaces, Journal of Membrane Science, 296 (2007) 29-41.
[31] B. Saini, M.K. Sinha, S.K. Dash, Mitigation of HA, BSA and oil/water emulsion fouling of PVDF Ultrafiltration Membranes by SiO2-g-PEGMA nanoparticles, Journal of Water Process Engineering, (2018).
[32] R. Pal, Techniques for measuring the composition (oil and water content) of emulsions—a state of the art review, Colloids and Surfaces A: Physicochemical and Engineering Aspects, 84 (1994) 141-193.
[33] I. Sadeghi, A. Aroujalian, A. Raisi, B. Dabir, M. Fathizadeh, Surface modification of polyethersulfone ultrafiltration membranes by corona air plasma for separation of oil/water emulsions, Journal of Membrane Science, 430 (2013) 24-36.
[34] R. Jamshidi Gohari, E. Halakoo, W.J. Lau, M.A. Kassim, T. Matsuura, A.F. Ismail, Novel polyethersulfone (PES)/hydrous manganese dioxide (HMO) mixed matrix membranes with improved anti-fouling properties for oily wastewater treatment process, RSC Advances, 4 (2014) 17587-17596.
[35] G. Arthanareeswaran, V.M. Starov, Effect of solvents on performance of polyethersulfone ultrafiltration membranes: Investigation of metal ion separations, Desalination, 267 (2011) 57-63.
[36] X. Zhao, Y. Su, J. Cao, Y. Li, R. Zhang, Y. Liu, Z. Jiang, Fabrication of antifouling polymer–inorganic hybrid membranes through the synergy of biomimetic mineralization and nonsolvent induced phase separation, Journal of Materials Chemistry A, 3 (2015) 7287-7295.
[37] G. Zhang, J. Jiang, Q. Zhang, X. Zhan, F. Chen, Amphiphilic poly (ether sulfone) membranes for oil/water separation: Effect of sequence structure of the modifier, AIChE Journal, 63 (2017) 739-750.
[38] V. Moghimifar, A.E. Livari, A. Raisi, A. Aroujalian, Enhancing the antifouling property of polyethersulfone ultrafiltration membranes using NaX zeolite and titanium oxide nanoparticles, Rsc Advances, 5 (2015) 55964-55976.
[39] H. Yamamura, K. Kimura, Y. Watanabe, Mechanism involved in the evolution of physically irreversible fouling in microfiltration and ultrafiltration membranes used for drinking water treatment, Environmental science & technology, 41 (2007) 6789-6794.
[40] J. Dickhout, J. Moreno, P. Biesheuvel, L. Boels, R. Lammertink, W. de Vos, Produced water treatment by membranes: A review from a colloidal perspective, Journal of colloid and interface science, 487 (2017) 523-534.
[41] Z. Wang, J. Ma, C.Y. Tang, K. Kimura, Q. Wang, X. Han, Membrane cleaning in membrane bioreactors: a review, Journal of membrane science, 468 (2014) 276-307.
[42] S.S. Madaeni, T. Mohamamdi, M.K. Moghadam, Chemical cleaning of reverse osmosis membranes, Desalination, 134 (2001) 77-82.

Supplementary information

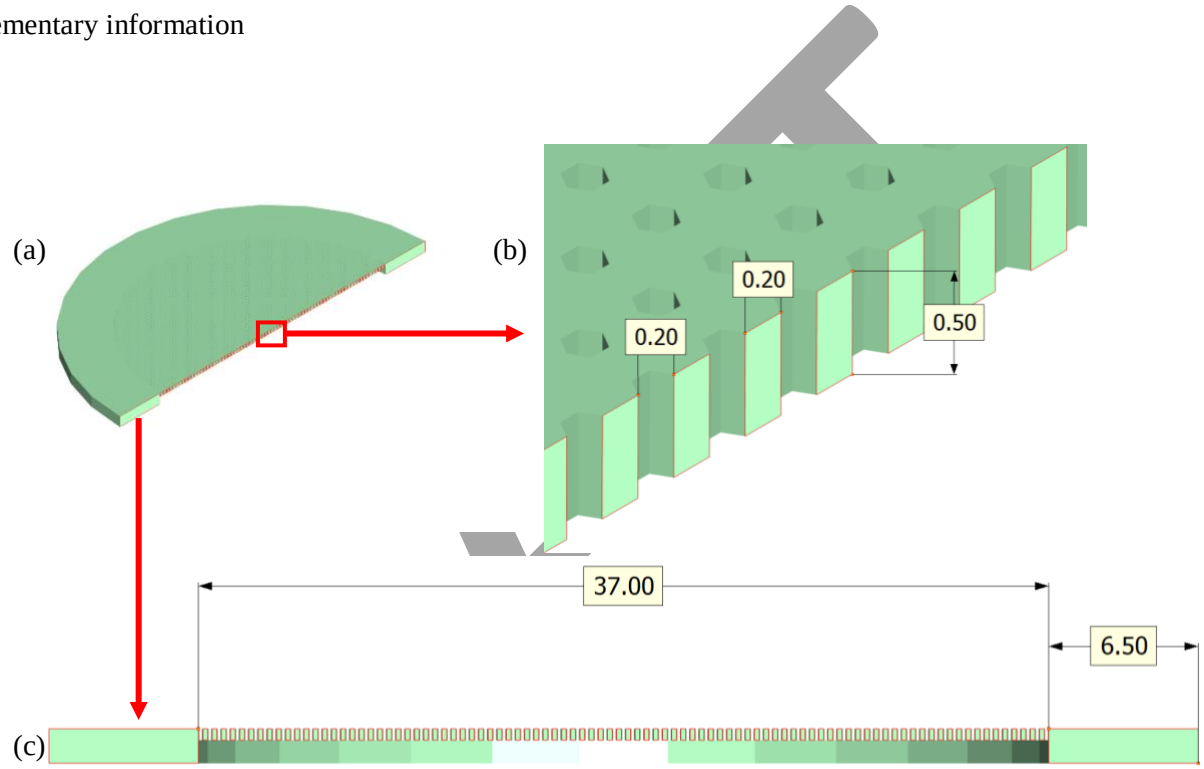

Fig. S 1. CAD of 3D flat support: (a) top view, (b) enlarged cross section, the pore diameter = 0.2 mm, the distance between pores = 0.2 mm and (c) side view, all dimensions are in mm.

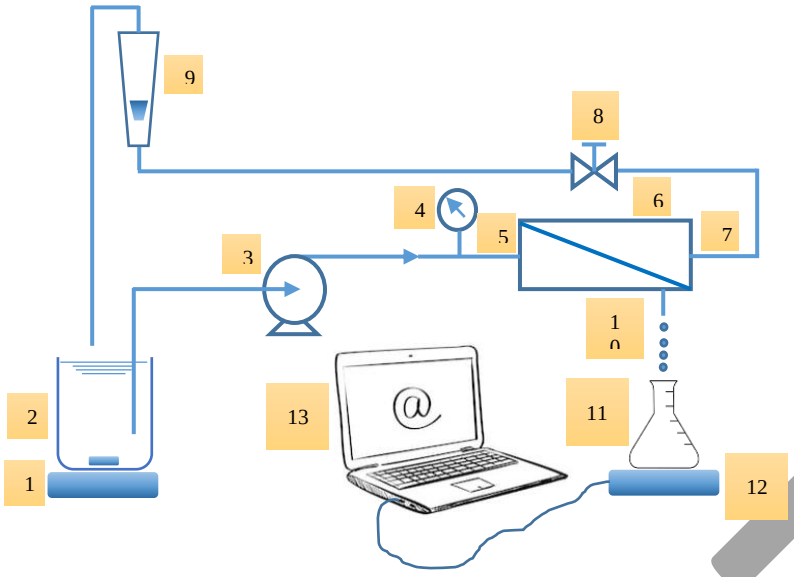

1. Magnetic stirrer
2. Feed tank
3. Gear pump
4. Pressure gauge
5. Feed input
6. Membrane module
7. Retentate
8. Valve
9. Rotameter
10. Permeate
11. Volumetric flask
12. Balance
13. Computer

Fig. S2. Schematic of the cross-flow filtration rig.

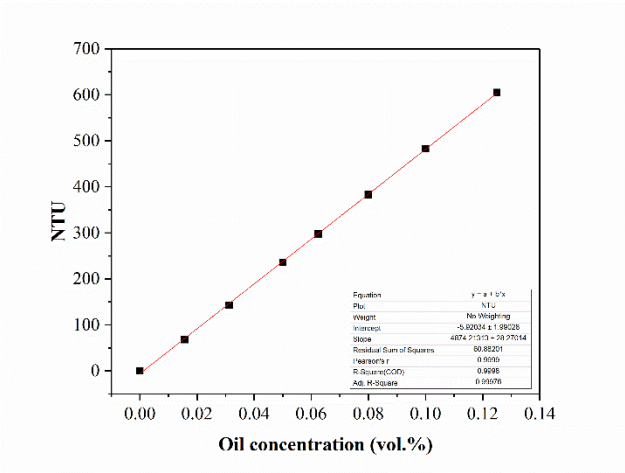

Fig. S3. Calibration curve of oil in water emulsions measured using Turbidity meter (*EUTECH TN-100, Thermo-Scientific*).

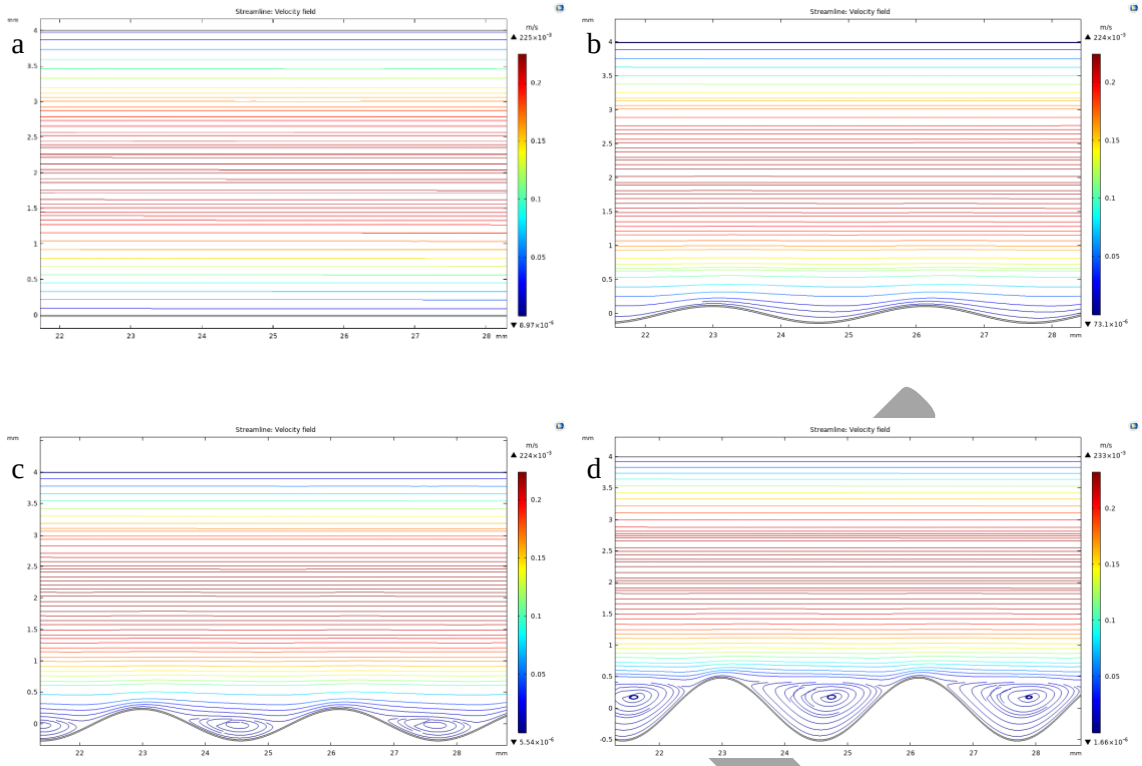

Fig. S4. Flow streamlines, Re = 1000, (a) flat, (b) peak height = 0.125 µm, (c) peak height = 0.25 µm, (d) peak height = 0.5 µm. Eddies region was expanded with the increase of the peak height at constant velocity.

Fig. S5. Oil in water emulsion (a) the permeate, (b) the feed before ultrafiltration process

Table S1. Differences between literature review and this study

	Modification process	Casting conditions		Compaction		Operating conditions		Oil in water emulsion		Membrane performance				Ref.
		rel. humidity (%)	temp. (°C)	pressure (bar)	time (min)	pressure (bar)	flowrate (L/min)	oil con. (mg/L)	Type of oil	permeance (LMH bar^{-1}) pure water	permeance (LMH bar^{-1}) o/w emulsion	FRR (%)	Oil rejection (%)	
NMP	Mixing with Hydrous manganese dioxide (nanoparticles)	---	---	1	30	1	---	1000	Crude	573.2	~ 100	75.4/ washing with pure water	100	[44]
NMP	Mixing with Cellulose acetate / polyethylene glycol	---	---	4	---	4	0.2	500	Kerosene	20.25	6.75	-----	88	[45]
DMF	Mixing with PEGMA and TFOA	---	---	1.5	30	1	Dead end cell	900	Vacuum	---	---	99.8 / washing with pure water	99.5	[38]
DMAc	Mixing with SiO2-g-(PDMAEMA-co-PDMAPS) nanoparticles	---	---	1.6	60	1	Dead end cell	900	Engine	172.30	79.83	84.26/ washing with pure water	100	[46]
DMAc	zwitterionic polymers from a reactive amphiphilic copolymer additive	---	---	2.5	30	2	Dead end cell	1500	---	74.5	---	99/ washing with pure water	~ 100	[47]
DMAc	Surface modification / corona air plasma	---	---	---	---	1.5	---	3000	Gas	108.46	37.86	---	98.2	[34]
DMF	Surface modification / corona plasma – assisted coating TiO_2 nanoparticles	---	---	---	---	1.5	---	3000	Gas	12.97	10.96	---	99	[48]
	Blending and surface coating by NaX zeolite and TiO_2 nanoparticles	---	---	---	---	1.5		3000	Gas	---	6.3	82.6/ washing with pure water	99.1	[49]
DMF	Mixing with Pluronic F127	---	---	1.5	30	1	Dead end cell	900	Soybean	---	82.98	93.33 / after chemical washing	100	[11]
DMAc	Wavy surface	30	19 – 21	1.5	90 - 120	1	1.4	2490	Sunflower	16 ± 0.46	3 ± 0.8	89 ± 2.7/ washing with pure water	96 ± 3	this study

where: **NMP:** N-Methyl-2-pyrrolidone and **DMF**: Dimethylformamide

[1] D.S. Sholl, R.P. Lively, Seven chemical separations to change the world, in: Nature, 2016, pp. 435-437.
[2] Y. Wei, H. Qi, X. Gong, S. Zhao, Specially Wettable Membranes for Oil–Water Separation, Advanced Materials Interfaces, 0 1800576.
[3] H.J. Tanudjaja, V.V. Tarabara, A.G. Fane, J.W. Chew, Effect of cross-flow velocity, oil concentration and salinity on the critical flux of an oil-in-water emulsion in microfiltration, Journal of Membrane Science, 530 (2017) 11-19.
[4] R. Moosai, R.A. Dawe, Gas attachment of oil droplets for gas flotation for oily wastewater cleanup, Separation and purification technology, 33 (2003) 303-314.
[5] R. Mohammed, A. Bailey, P. Luckham, S. Taylor, Dewatering of crude oil emulsions 3. Emulsion resolution by chemical means, Colloids and Surfaces A: Physicochemical and Engineering Aspects, 83 (1994) 261-271.

[6] S. Maiti, I. Mishra, S. Bhattacharya, J. Joshi, Removal of oil from oil-in-water emulsion using a packed bed of commercial resin, Colloids and Surfaces A: Physicochemical and Engineering Aspects, 389 (2011) 291-298.
[7] M.-J. Um, S.-H. Yoon, C.-H. Lee, K.-Y. Chung, J.-J. Kim, Flux enhancement with gas injection in crossflow ultrafiltration of oily wastewater, Water research, 35 (2001) 4095-4101.
[8] M. Padaki, R. Surya Murali, M.S. Abdullah, N. Misdan, A. Moslehyani, M.A. Kassim, N. Hilal, A.F. Ismail, Membrane technology enhancement in oil–water separation. A review, Desalination, 357 (2015) 197-207.
[9] S. Kasemset, A. Lee, D.J. Miller, B.D. Freeman, M.M. Sharma, Effect of polydopamine deposition conditions on fouling resistance, physical properties, and permeation properties of reverse osmosis membranes in oil/water separation, Journal of Membrane Science, 425-426 (2013) 208-216.
[10] I.W. Cumming, R.G. Holdich, I.D. Smith, The rejection of oil by microfiltration of a stabilised kerosene/water emulsion, Journal of Membrane Science, 169 (2000) 147-155.
[11] W. Chen, J. Peng, Y. Su, L. Zheng, L. Wang, Z. Jiang, Separation of oil/water emulsion using Pluronic F127 modified polyethersulfone ultrafiltration membranes, Separation and Purification Technology, 66 (2009) 591-597.
[12] S. Lee, Y. Aurelle, H. Roques, Concentration polarization, membrane fouling and cleaning in ultrafiltration of soluble oil, Journal of Membrane Science, 19 (1984) 23-38.
[13] M. Hlavacek, Break-up of oil-in-water emulsions induced by permeation through a microfiltration membrane, Journal of membrane science, 102 (1995) 1-7.
[14] R. Zolfaghari, A. Fakhru'l-Razi, L.C. Abdullah, S.S. Elnashaie, A. Pendashteh, Demulsification techniques of water-in-oil and oil-in-water emulsions in petroleum industry, Separation and Purification Technology, 170 (2016) 377-407.
[15] Y. Ding, S. Maruf, M. Aghajani, A.R. Greenberg, Surface patterning of polymeric membranes and its effect on antifouling characteristics, Separation Science and Technology, 52 (2017) 240-257.
[16] S.H. Maruf, L. Wang, A.R. Greenberg, J. Pellegrino, Y. Ding, Use of nanoimprinted surface patterns to mitigate colloidal deposition on ultrafiltration membranes, Journal of membrane science, 428 (2013) 598-607.
[17] W. Choi, E.P. Chan, J.-H. Park, W.-G. Ahn, H.W. Jung, S. Hong, J.S. Lee, J.-Y. Han, S. Park, D.-H. Ko, Nanoscale pillar-enhanced tribological surfaces as antifouling membranes, ACS applied materials & interfaces, 8 (2016) 31433-31441.
[18] J.W. Bae, Y.-H. Cho, Y.-E. Sung, K. Shin, J.Y. Jho, Performance enhancement of polymer electrolyte membrane fuel cell by employing line-patterned Nafion membrane, Journal of Industrial and Engineering Chemistry, 18 (2012) 876-879.
[19] D.-C. Choi, S.-Y. Jung, Y.-J. Won, J.H. Jang, J.-W. Lee, H.-R. Chae, J. Lim, K.H. Ahn, S. Lee, J.-H. Kim, Effect of Pattern Shape on the Initial Deposition of Particles in the Aqueous Phase on Patterned Membranes during Crossflow Filtration, Environmental Science & Technology Letters, 4 (2017) 66-70.
[20] L. Vogelaar, J.N. Barsema, C.J. van Rijn, W. Nijdam, M. Wessling, Phase separation micromolding—PSμM, Advanced materials, 15 (2003) 1385-1389.
[21] R.J. Gohari, W. Lau, T. Matsuura, A. Ismail, Effect of surface pattern formation on membrane fouling and its control in phase inversion process, Journal of membrane science, 446 (2013) 326-331.
[22] Y.-J. Won, S.-Y. Jung, J.-H. Jang, J.-W. Lee, H.-R. Chae, D.-C. Choi, K.H. Ahn, C.-H. Lee, P.-K. Park, Correlation of membrane fouling with topography of patterned membranes for water treatment, Journal of Membrane Science, 498 (2016) 14-19.
[23] Y.K. Lee, Y.-J. Won, J.H. Yoo, K.H. Ahn, C.-H. Lee, Flow analysis and fouling on the patterned membrane surface, Journal of membrane science, 427 (2013) 320-325.
[24] M. Xie, W. Luo, S.R. Gray, Surface pattern by nanoimprint for membrane fouling mitigation: Design, performance and mechanisms, Water research, 124 (2017) 238-243.
[25] O. Heinz, M. Aghajani, A.R. Greenberg, Y. Ding, Surface-patterning of polymeric membranes: fabrication and performance, Current Opinion in Chemical Engineering, 20 (2018) 1-12.

[26] Z.-X. Low, Y.T. Chua, B.M. Ray, D. Mattia, I.S. Metcalfe, D.A. Patterson, Perspective on 3D printing of separation membranes and comparison to related unconventional fabrication techniques, Journal of Membrane Science, 523 (2017) 596-613.
[27] T. Femmer, A.J. Kuehne, J. Torres-Rendon, A. Walther, M. Wessling, Print your membrane: Rapid prototyping of complex 3D-PDMS membranes via a sacrificial resist, Journal of Membrane Science, 478 (2015) 12-18.
[28] S. Yuan, D. Strobbe, J.-P. Kruth, P. Van Puyvelde, B. Van der Bruggen, Super-hydrophobic 3D printed polysulfone membranes with a switchable wettability by self-assembled candle soot for efficient gravity-driven oil/water separation, Journal of Materials Chemistry A, 5 (2017) 25401-25409.
[29] S. Badalov, Y. Oren, C.J. Arnusch, Ink-jet printing assisted fabrication of patterned thin film composite membranes, Journal of Membrane Science, 493 (2015) 508-514.
[30] N.C. Wardrip, M. Dsouza, M. Urgun-Demirtas, S.W. Snyder, J.A. Gilbert, C.J. Arnusch, Printing-Assisted Surface Modifications of Patterned Ultrafiltration Membranes, ACS Applied Materials & Interfaces, 8 (2016) 30271-30280.
[31] Y.M.J. Chew, W.R. Paterson, D.I. Wilson, Fluid dynamic gauging: A new tool to study deposition on porous surfaces, Journal of Membrane Science, 296 (2007) 29-41.
[32] B. Saini, M.K. Sinha, S.K. Dash, Mitigation of HA, BSA and oil/water emulsion fouling of PVDF Ultrafiltration Membranes by SiO2-g-PEGMA nanoparticles, Journal of Water Process Engineering, (2018).
[33] R. Pal, Techniques for measuring the composition (oil and water content) of emulsions—a state of the art review, Colloids and Surfaces A: Physicochemical and Engineering Aspects, 84 (1994) 141-193.
[34] I. Sadeghi, A. Aroujalian, A. Raisi, B. Dabir, M. Fathizadeh, Surface modification of polyethersulfone ultrafiltration membranes by corona air plasma for separation of oil/water emulsions, Journal of Membrane Science, 430 (2013) 24-36.
[35] R. Jamshidi Gohari, E. Halakoo, W.J. Lau, M.A. Kassim, T. Matsuura, A.F. Ismail, Novel polyethersulfone (PES)/hydrous manganese dioxide (HMO) mixed matrix membranes with improved anti-fouling properties for oily wastewater treatment process, RSC Advances, 4 (2014) 17587-17596.
[36] G. Arthanareeswaran, V.M. Starov, Effect of solvents on performance of polyethersulfone ultrafiltration membranes: Investigation of metal ion separations, Desalination, 267 (2011) 57-63.
[37] X. Zhao, Y. Su, J. Cao, Y. Li, R. Zhang, Y. Liu, Z. Jiang, Fabrication of antifouling polymer–inorganic hybrid membranes through the synergy of biomimetic mineralization and nonsolvent induced phase separation, Journal of Materials Chemistry A, 3 (2015) 7287-7295.
[38] G. Zhang, J. Jiang, Q. Zhang, X. Zhan, F. Chen, Amphiphilic poly (ether sulfone) membranes for oil/water separation: Effect of sequence structure of the modifier, AIChE Journal, 63 (2017) 739-750.
[39] V. Moghimifar, A.E. Livari, A. Raisi, A. Aroujalian, Enhancing the antifouling property of polyethersulfone ultrafiltration membranes using NaX zeolite and titanium oxide nanoparticles, Rsc Advances, 5 (2015) 55964-55976.
[40] H. Yamamura, K. Kimura, Y. Watanabe, Mechanism involved in the evolution of physically irreversible fouling in microfiltration and ultrafiltration membranes used for drinking water treatment, Environmental science & technology, 41 (2007) 6789-6794.
[41] J. Dickhout, J. Moreno, P. Biesheuvel, L. Boels, R. Lammertink, W. de Vos, Produced water treatment by membranes: A review from a colloidal perspective, Journal of colloid and interface science, 487 (2017) 523-534.
[42] Z. Wang, J. Ma, C.Y. Tang, K. Kimura, Q. Wang, X. Han, Membrane cleaning in membrane bioreactors: a review, Journal of membrane science, 468 (2014) 276-307.
[43] S.S. Madaeni, T. Mohamamdi, M.K. Moghadam, Chemical cleaning of reverse osmosis membranes, Desalination, 134 (2001) 77-82.

[44] R.J. Gohari, E. Halakoo, W.J. Lau, M.A. Kassim, T. Matsuura, A.F. Ismail, Novel polyethersulfone (PES)/hydrous manganese dioxide (HMO) mixed matrix membranes with improved anti-fouling properties for oily wastewater treatment process, RSC Advances, 4 (2014) 17587-17596.
[45] A. Mansourizadeh, A.J. Azad, Preparation of blend polyethersulfone/cellulose acetate/polyethylene glycol asymmetric membranes for oil–water separation, Journal of Polymer Research, 21 (2014) 375.
[46] J. Yin, J. Zhou, Novel polyethersulfone hybrid ultrafiltration membrane prepared with SiO2-g-(PDMAEMA-co-PDMAPS) and its antifouling performances in oil-in-water emulsion application, Desalination, 365 (2015) 46-56.
[47] Y.-F. Zhao, P.-B. Zhang, J. Sun, C.-J. Liu, Z. Yi, L.-P. Zhu, Y.-Y. Xu, Versatile antifouling polyethersulfone filtration membranes modified via surface grafting of zwitterionic polymers from a reactive amphiphilic copolymer additive, Journal of colloid and interface science, 448 (2015) 380-388.
[48] V. Moghimifar, A. Raisi, A. Aroujalian, Surface modification of polyethersulfone ultrafiltration membranes by corona plasma-assisted coating TiO2 nanoparticles, Journal of Membrane Science, 461 (2014) 69-80.
[49] X. Ma, Y. Su, Q. Sun, Y. Wang, Z. Jiang, Enhancing the antifouling property of polyethersulfone ultrafiltration membranes through surface adsorption-crosslinking of poly (vinyl alcohol), Journal of Membrane Science, 300 (2007) 71-78.